Improving the overall thermal performance of parabolic trough solar collectors using porous media

19th International Conference on Renewable Energies and Power Quality (ICREPQ'21)
Almeria (Spain), 28th to 30th July 2021
Renewable Energy and Power Quality Journal (RE&PQJ)
ISSN 2172-038 X, Volume No.19, September 2021

Improving the overall thermal performance of parabolic trough solar collectors using porous media

H. Ebadi[1], A. Cammi[2], and L. Savoldi[1*]

[1] MAHTEP Group, Dipartimento Energia "Galileo Ferraris" (DENERG),
Politecnico di Torino, Italy
Corso Duca degli Abruzzi 24, 10129 Torino (Italy)
Phone/Fax number:+39 011 090 4559, e-mail: laura.savoldi@polito.it
[2] Department of Energy
Politecnico di Milano (Italy)

Abstract. The use of a porous insert constituted by a metal matrix of copper Raschig Rings is proposed here for parabolic trough solar collectors. The CFD analysis, based on a well-established numerical model, allows computing a significant increase in the thermal performance of the tube considered in the analysis, when equipped with the porous insert, with respect to a smooth pipe. The useful power grows up to ~96 % of the absorbed incident power. A reduction of a factor of 5 in the radiative and convective losses is computed, due to a large drop in the pipe surface temperature. The length of the porous insert, however, should be carefully evaluated in view of the significant additional pressure drop caused by the insert.

Keywords. Solar PTC, CFD, Thermal modeling, Rachig rings, Porous.

1. Introduction

The use of solar energy is one of the most effective ways to solve recent energy problems, which are associated with global warming, declining fossil fuels, and rising electricity prices [1]. Solar energy is an abundant renewable energy source that can be converted into useful heat and electricity. Therefore, solar energy can be considered as a reliable and suitable source of energy for various applications, ranging from domestic water heating to solar drying and solar power plants [2,3]. Generally, a solar collector converts solar radiation into heat and transfers the heat to a working fluid which can be air, water, oil, or other fluids. The obtained thermal energy can be used in a variety of applications. Solar collectors come in several types including flat-plate collectors (FPCs), parabolic trough collectors (PTCs), compound parabolic collectors (CPCs), and Fresnel lenses. The PTC is one of the most prominent and promising technologies used to convert solar radiation into useful heat [4]. A PTC mainly consists of a highly polished surface as the reflector which might be an aluminum surface with a reflection of 88.5% to 95% or any highly-reflective mirrors. When solar radiation incidents on the aperture of the concentrator, the sun rays are reflected on the absorber, which is located on the central axis of the collector. Figure 1 shows the main components of a PTC [5,6].

In the focal area, a tubular absorber is centered around a glass cover, which is located at a distance from the absorber, and is free of air or filled with air. This glass cover helps to reduce heat losses [5]. The tube absorber is held in place by two retainers on both sides so that the adsorbent does not have a problem due to the weight of the working fluid, wind, and the weight of the absorber structure. The most common materials that are used as a light-reflecting surface are aluminum or steel sheets [8]. Concentrators are the most suitable solar collectors that can be used to achieve medium to high-temperature levels (more than 150°C) with the high thermal performance [9]. Among solar collectors technologies developed to harness the energy that comes from the sun, PTC is one of the most widely used solar collectors [10]. Typically, PTCs use a variety of heat transfer fluids (HTFs) such as air, CO2, nitrogen, and helium, and over the years a variety of methods have been employed to increase the temperature HTFs and therefore improve the overall thermal performance [11]. The main intention behind all previously conducted studies is to improve the heat transfer rate between the adsorbent and the working fluid as well as to increase the heat transfer coefficient or

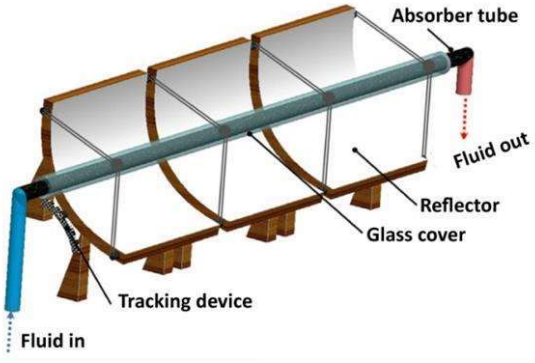

Figure 1. The main layout of a parabolic trough collector [7].

film coefficient. Also, increasing thermal performance leads to a decrease in the temperature gradient of the adsorbent, which reduces the likelihood of problems such as deformation in the adsorption of the tube [10,12]. Many studies have been conducted to investigate nanofluids to increase the thermal performance of PTCs [13]. Based on the literature review, porous inserts is one of the most-effective, cheap and available techniques to boost thermal performance in PTC systems. However, when porous materials are used in the flow direction of HTF, there is a pressure drop in the system which requires higher pumping power. Recently, a novel porous matrix with enhanced hydraulic properties was proposed by scientists [14,15], where Raschig Rings (RR) are used as the main element to produce the porous structure. This concept, although well known in chemical reactors, is very promising [16] and needs more investigations on its application for various purposes, especially for advancing CSP technology. Therefore, this research aims to reveal some thermohydraulic behaviors of this technology under CSP-relevant operational conditions to pave the way for further research and development. To this end, a numerical investigation was carried out using CFD codes through the implementation of commercial software Star CCM+ (V. 2020.1.1) for simulating a PTC solar absorber modified with RR as the porous medium. To assess the system performance, a PTC thermal heat load was applied to the model using data in the literature. Results were evaluated in the case of heat thermal losses for both absorber tube and glass envelope, comparing the smooth tube with the enhanced tube.

2. Model setup

2.1. Parabolic trough collector

A conventional tubular absorber with a cylindrical geometry, the most common type used in PTC applications, is considered in this study. Moreover, an evacuated glass envelope is also taken into account to simulate the PTC operation. Dimensions (diameter, thickness, length) are selected based on the previous studies [16] conducted in the Plataforma Solar de Almeria to make the results comparable and applicable for real scale systems. Therefore, the tube was designed with an inner diameter was set as 20.6 mm, and an outer diameter of 25.4 mm, made of Inconel (emissivity=0.26). While the glass enveloped was developed as 30 mm inner diameter and 32 mm outer diameter made of standard glass (emissivity=0.86). Two different options were considered: a plain smooth pipe (SP) and a pipe with a RR insert with a length of 6 cm (RP), beginning 7.5 cm downstream of the inlet. As far as the thermal driver is concerned, the heat load was simulated using data of local concentration ratio (LCR) in literature [17], and results are plotted in Fig. 2. As a result, the total solar incident on the PTC was obtained with the following relation.

$$\boldsymbol{S = LCR \times IAM \times DNI} \quad (1)$$

Where DNI is the maximum solar incident (W/m^2) and is equal to 1000 W/m^2, and IAM is the incident angle modifier which was considered to be 1 in this study due to the assumption of the 0 incident angle (θ). Thus, the total energy received on the wall of both pipes is 0.314 kW.

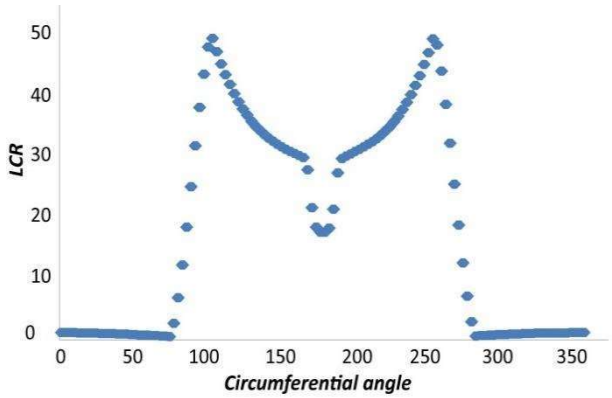

Figure 2. The local concentration ratio on the outer surface of the tube.

Dry air with temperature-dependent thermophysical properties was chosen as the gaseous working fluid with in a total flow rate of 40 l/min, comparable to that in [16].

2.2. Porous media preparation

The integration of DEM simulation in the selected case-study led to the development of the porous matrix consisting of RR, following the procedure introduced by Allio et al. [14]. This process was conducted in three stages in which firstly a container as the bulk volume of the matrix was devised and solid cylinders with the same dimensions as RR were injected along the gravity to fill the container. The transient DEM simulation was continued until the number of cylinders reached the desired value which was obtained based on the target porosity of 78.8% [14]. In the following step, solid particles were replaced with hollow rings to form a cylindrical matrix with 60 mm length, consisting of RR. Copper with an effective thermal conductivity of 2600 W/m/K [15] was selected as the RR material. Figure 3 represent the 3D model produced as a 60 mm RR porous media through the procedure described.

2.3. Numerical approach

Simulations were carried out based on a thermo-hydraulic model developed in the commercial Star CCM+ software implementing a three-dimensional analysis with steady-state, turbulent flow conditions. A steady-state conjugate heat transfer model was used to study the thermal behaviour between solid and fluid regions. Radiation boundary condition with face-to-face model [18] was applied to the surfaces of pipe and glass envelope to simulate the heat exchange between these element.

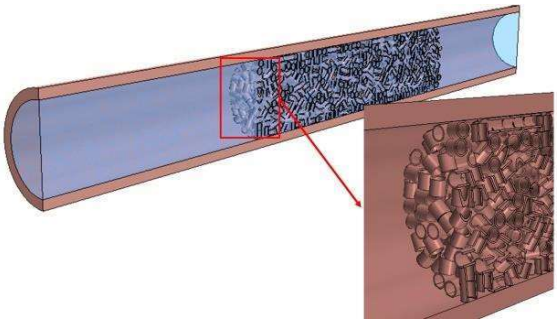

Figure 3. Geometry developed for the enhanced tube with RR.

The thermal model was performed based on several energy balance equations developed for PTC elements. As presented below, the energy balance relation on the glass envelope was given as;

$$\boldsymbol{q_{s-g} + q_{C,a-g} + q_{r,a-g} = q_{C,g-amb} + q_{r,g-amb}} \quad (2)$$

Where $\boldsymbol{q_{s-g}}$ represent the solar energy absorbed by the glass envelope, $\boldsymbol{q_r}$ is the radiation heat, $\boldsymbol{q_C}$ is the convection, and $\boldsymbol{g}$, $\boldsymbol{a}$ and $\boldsymbol{amb}$ indicate glass, absorber, and ambient, respectively. It is noteworthy to mention that since the configuration of PTC absorber was assumed to be an evacuated tube, the convection loss between the absorber and glass envelope was set as 0 in the simulations. Moreover, for the convection loss from the absorber to the ambient a constant heat transfer coefficient of 10 W/m^{2}K was imposed in the simulation (i.e., the external air field was not simulated). Also, the energy balance relation on the absorber tube was computed as below.

$$\boldsymbol{q_{s-a} = q_{C,f-a} + q_{C,a-g} + q_{r,a-g}} \quad (3)$$

In (3), $q_{C,f-a}$ is the useful heat that is transferred to the HTF (f), and q_{s-a} accounts for the solar energy transmitted through the envelope and absorbed by the absorber tube, as given in (4).

$$\boldsymbol{q_{s-a} = S \times \eta_{opt,max} \times cos\,(\theta)} \quad (4)$$

Where $\eta_{opt,max}$ (set to 0.78 based on the literature [19]) is the maximum optical efficiency of the PTC, which includes the absorption of the absorber, glass transmission, overall intercept factor.

The solid regions, where a segregated solid energy equation was solved, consists of the glass and pipe with related thermophysical properties such as thermal conductivity, specific heat, and density taken as functions of temperature. It is noteworthy to mention that, for the RP, the solid domain was built combining the RR geometries and their contact points with the pipe structure where later heat flux functions were applied as boundary condition at the outer wall.

The fluid region was formed by boolean subtraction of the matrix structure from a cylindrical geometry filled inside the tube. In order to simulate a turbulent flow inside the receiver, a two-equations Reynolds-Averaged Navier-Stokes (RANS) model, and namely the two-layer realizable κ-ε model, was used, with an all-y+ treatment at the wall. The two-layer version of the κ-ε model adds flexibility to the wall treatment switching automatically between low-y+ and high-y+ treatments. As indicated by Dixon et al., [20], the superiority of the realizable k-ε over the standard k-ε model refers to the addition of an improved equation for the turbulent energy dissipation rate ε, with a variable viscosity coefficient Cμ instead of a constant value. The main benefit of the realizable κ-ε model over standard κ-ε models was firstly introduced by Shih et al. [21], where C_μ is a function of mean strain and rotation rates, the angular velocity of the system rotation, and the turbulence fields κ-and ε [22]. Thus, as long as rotation boundary layers under strong adverse pressure gradients, separation, and recirculation with strong curvature are considered, similar to those found in packed tube simulation [23,24], this model could result in a reasonable performance. While the κ-ε turbulence model is widely used in the modeling of solar tubular absorber enhanced with inserts [25–29], it has been verified that, in the simulation of the tube equipped with RR, the use of the κ-ω SST model, already adopted in Savoldi et al. [15], could change the average temperature increase of the wall by 2%, which does not significantly affect the qualitative pictures that are presented below. As this study showed, the two models give comparable results for the case at hand, however, for a proper selection among the two, the accurate experimental data for model validation are necessary, which are not available at present. A reference pressure of 10 bar was set for the first segment, while boundary conditions for two models on the secondary segment were periodic constant mass flow rate (fully developed). To be sure to have fully developed flow at the pipe inlet for both SP ad RP, a 50 cm long smooth pipe with the same transverse dimensions was first simulated, and the outlet velocity were used as inlet conditions for the two options considered in this study. Thermal analysis was performed using a segregated flow temperature model and the boundary conditions of the secondary simulations were adjusted by the mean bulk temperature obtained at the outlet of the first segment (400.6 K).

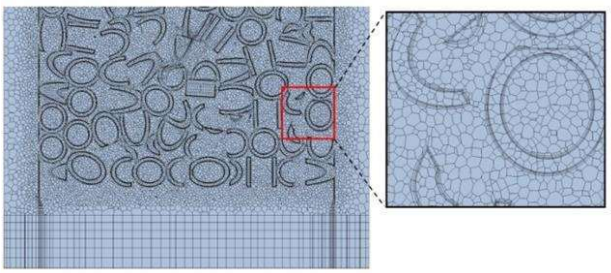

Figure 4. Mesh developed for the simulation of tube with RR.

In the meshing stage, polyhedral-based cells with a base size of 0.6 mm to a minimum limit of 0.06 mm were adopted in the RR region. The number of prism layers was set to 5 with y+ at the wall ~1 to make the model able to predict the sharp gradients on the wall boundaries. Inside the RR matrix the base size was reduced to 0.16 mm and the number of prism layers to 3. The portion of the plain pipe before and after the RR region was meshed extruding the mesh of the RR region. The result is a mesh based on prismatic cells with a polygonal base. As a result, more than 14.3 million cells were produced. Figure 4 illustrates the structure of the mesh developed for simulations in this study, with particular emphasis on the RR region.

3. Results and discussion

3.1. Hydraulic performance

Figure 5 illustrates the velocity fields obtained through the test cases carried out on the secondary segments. As expected, the porous insert produces high resistance to the flow which will increase the contact area between the solid and fluid parts. The arbitrary orientation of the rings could also accelerate the airflow in the void area and spaces with the sharp corner of rings. According to figure 5, air velocity rises to near 19 m/s within the porous regime. When the air leaves the porous region, there are some air streams with improved velocity that causes thermal mixing. It is noteworthy to mention that the obtained results can be affected by the applied heat and this must be taken into consideration for further analyses.

From the simulations, the amount of pressure is being lost through the porous region is significantly large (14 kPa) compared to those of the smooth pipe with 9.54 Pa (not shown) and will require an additional pumping energy to induce the flow.

3.2. Thermodynamic performance

Figure 6 presents the development of the temperature in the elements of the solar collector through the SP. In order to monitor the thermal performance of the solar collector, 4 different lines were created to extract the tube wall

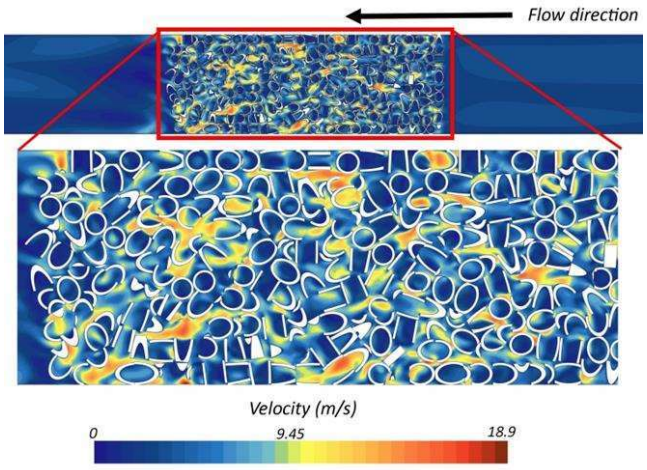

Figure 5. The air velocity field through (A) smooth pipe, (B) pipes with RR insert.

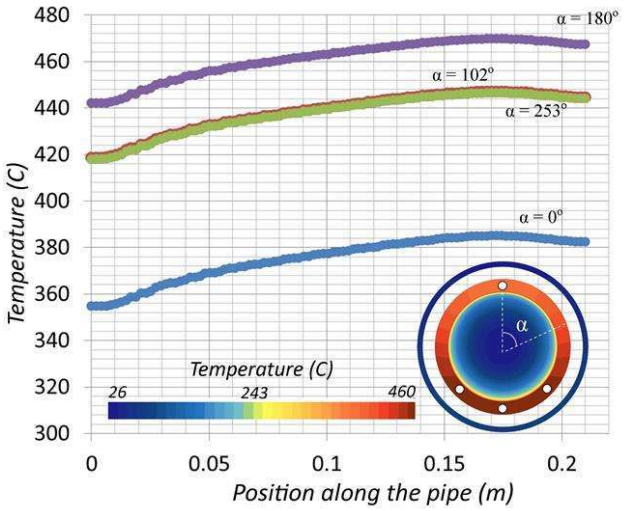

Figure 6. Temperature distribution on the wall of the smooth tube along the pipe length.

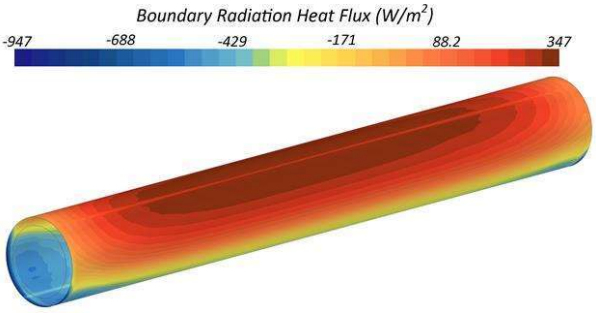

Figure 7. Radiation heat flux on the outer surface of the smooth pipe.

temperature with respect to the tube length. As depicted in the figure, derivative lines were selected based on top and bottom sections as well as the positions where the solar intensity is the maximum. Thus, the bottom section of the tube undergoes the maximum temperature increase due to the non-uniformity in solar load. The high temperature values reveal that the heat dissipation from the absorber wall is weak and this contributes to high heat loss from the receiver, and glass leading to low thermal efficiency in solar systems. Simulation data also shows that tube wall temperature increases as the air gets heated and the heat transfer rate decreases, where the line with $\alpha = 180^{o}$ shows the maximum temperature as $470^{o}C$ occurred at the bottom section of the tube. The two lateral lines ($\alpha = 102$ and 253^{o}) represent a constant behavior, with a middle-temperature rise to $440^{o}C$. The upper section which receives the minimum solar radiation (equal to the absolute value of DNI), has the smallest temperature rise with $385^{o}C$, and consequently shows the minimum contribution to heat loss from the solar collector.

What is also highlighted in figure 6 is the short temperatures falls that happen near the two boundary faces. This behavior can be traced back to the features of radiation model which is based on the ray-tracing approach and results in the loss of a fraction of heat by emitting rays to the ambient at the areas near to the ends.

Figure 7 proves such behavior in term of the radiation on the outer surface of the smooth tube. Please note that the negative values present the flux leaving the surface.

Figure 8 provides the temperature distribution on the wall of the tube associated with a 6 cm RR porous media. From the figure, the porous insert can reduce the wall temperature all around the tube, where the maximum reduction in the temperature rise happens at the lower section with nearly 82% at X=0.24 m. This strongly demonstrates the improving effects of the RR insert in the heat transfer, which can be attributed to heat conduction that takes between the tube wall and RR matrix and this grows the heat transfer area to a greater extent. Thus, air could absorb a higher amount of heat passing through the heated rings and make the walls cooler. What is also evidenced in figure 8 is the thermal mixing effect produced by the arbitrary structure of the RR. As a result, when the air leaves the porous media, the chaotic situation of air streamlines results in the enhanced convective heat transfer coefficients which increases the heat removal downstream compared to smooth pipe. That is why the temperature reduction continues to some extent after the porous zone, see also figure 9. Although the sidewalls start to heat up again, the new temperature growth has a slight trend due to the improved heat transfer downstream of the RR region.

One of the drawbacks that accounts for such porous media

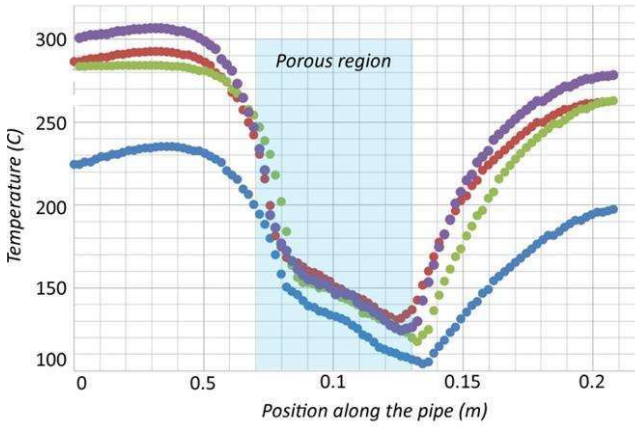

Figure 8. Temperature profile of the wall of the tube enhanced with RR insert.

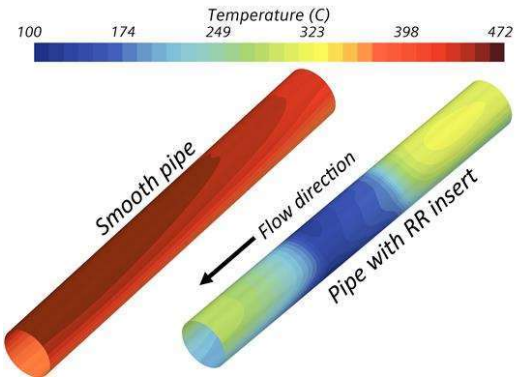

Figure 9. Comparison of tube wall temperatures for the two cases of SP (left) and RP (right) – view of the heated side.

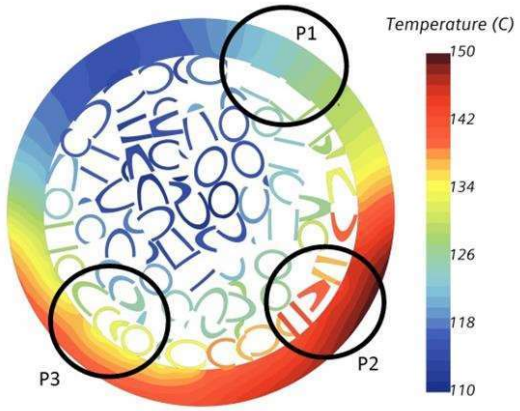

Figure 10. Temperature distribution of the cross section of the tube associated with RR at X=0.1 m (test case 3)

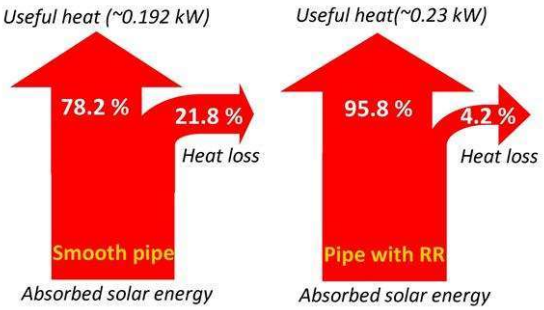

Figure 11. Sankey diagram for the thermal power receiving the smooth and enhanced pipes.

is the randomness of the rings at the outermost layer which does not guarantee the perfect contact with the tube wall. In this regard, figure 10 indicates the temperature distribution between the RR and tube and how heat is transferred through the contacts. As shown, when the orientation of the rings is such that the air cannot flow through them (P1), wall temperature increases locally and the neighboring layers in azimuthal direction remain ineffective in terms of heat transfer. Also in (P2) the ring rests perpendicular to the flow direction (tube axis) air stagnation happens and rings start heating up without the effective role in heat dissipation through other rings. As opposed to that, when the wall of the rings touches the tube wall, heat transfer increases not only due to the proper contacts but also for the reason of air passage through the rings orifices parallel to the flow direction (P3). As a result, despite the symmetrical heat load applied to the PTC solar absorber, such porous media could cause some asymmetrical temperature distributions along with the tube length corresponding to the structure of the ring at the outermost layer.

To elaborate on the enhancement effect of the RR insert, radiation heat loss from the absorber was determined based on the average temperature of the tube and glass cover. As shown in figure 11, the total solar energy transmitted through the glass cover and reaches the absorber will be transferred to the fluid effectively as 78.2 and 95.8% in the case of smooth and enhanced pipe. The reason for such gap refers to temperature mitigations

on the wall of the tube with RR in which the higher heat transfer area and thermal mixing triggered a larger heat exchange between the solid and the fluid.

4. Conclusions and perspective

A CFD analysis was performed on the enhancing effects of a novel porous media consisting of RR and incorporated with a solar PTC absorber. Thermal performance was investigated through a series of simulations where 2 models were developed for pipe with both smooth and enhanced configurations. Results demonstrated that when the porous media is employed pressure drop increases to 14 kPa. Giving the higher heat transfer area between the solid and fluid parts, the RR insert improves the total useful energy to almost 96% of the absorbed power and diminishes the hotspot on the wall of the tube up to 82%. Further works are needed to investigate other thermal characteristics and optimization criteria for a better deployment of this technology into solar applications.

Acknowledgements

We acknowledge the use of the computational resources provided by hpc@polito, which is a project of Academic Computing within the Department of Control and Computer Engineering at the Politecnico di Torino (http://hpc.polito.it).

References

[1] E. Casati, F. Casella, P. Colonna, Design of CSP plants with optimally operated thermal storage, Sol. Energy. 116 (2015) 371–387. https://doi.org/10.1016/j.solener.2015.03.048.

[2] R. Tripathi, G.N. Tiwari, Energetic and exergetic analysis of N partially covered photovoltaic thermal-compound parabolic concentrator (PVT-CPC) collectors connected in series, Sol. Energy. 137 (2016) 441–451. https://doi.org/10.1016/j.solener.2016.08.048.

[3] Y. Qiu, Y.L. He, P. Li, B.C. Du, A comprehensive model for analysis of real-time optical performance of a solar power tower with a multi-tube cavity receiver, Appl. Energy. 185 (2017) 589–603. https://doi.org/10.1016/j.apenergy.2016.10.128.

[4] B. El Ghazzani, D. Martinez Plaza, R. Ait El Cadi, A. Ihlal, B. Abnay, K. Bouabid, Thermal plant based on parabolic trough collectors for industrial process heat generation in Morocco, Renew. Energy. 113 (2017) 1261–1275. https://doi.org/10.1016/j.renene.2017.06.063.

[5] SCHOTT, SCHOTT PTR 70 Receiver, (1992).

[6] W. Fuqiang, C. Ziming, T. Jianyu, Y. Yuan, S. Yong, L. Linhua, Progress in concentrated solar power technology with parabolic trough collector system: A comprehensive review, Renew. Sustain. Energy Rev. 79 (2017) 1314–1328. https://doi.org/10.1016/j.rser.2017.05.174.

[7] S. Suman, M.K. Khan, M. Pathak, Performance enhancement of solar collectors - A review, Renew. Sustain. Energy Rev. 49 (2015) 192–210. https://doi.org/10.1016/j.rser.2015.04.087.

[8] S.A. Murtuza, H.V. Byregowda, M.M.A. H, M. Imran, Experimental and simulation studies of parabolic trough collector design for obtaining solar energy, Resour. Technol. 3 (2017) 414–421. https://doi.org/10.1016/j.reffit.2017.03.003.

[9] A. Fernández-García, E. Zarza, L. Valenzuela, M. Pérez, Parabolic-trough solar collectors and their applications, Renew. Sustain. Energy Rev. 14 (2010) 1695–1721. https://doi.org/10.1016/j.rser.2010.03.012.

[10] Y. Wang, J. Xu, Q. Liu, Y. Chen, H. Liu, Performance analysis of a parabolic trough solar collector using Al2O3/synthetic oil nanofluid, Appl. Therm. Eng. 107 (2016) 469–478. https://doi.org/10.1016/j.applthermaleng.2016.06.170.

[11] E. Bellos, C. Tzivanidis, I. Daniil, K.A. Antonopoulos, The impact of internal longitudinal fins in parabolic trough collectors operating with gases, Energy Convers. Manag. 135 (2017) 35–54. https://doi.org/10.1016/j.enconman.2016.12.057.

[12] J. Muñoz, A. Abánades, Analysis of internal helically finned tubes for parabolic trough design by CFD tools, Appl. Energy. 88 (2011) 4139–4149. https://doi.org/10.1016/j.apenergy.2011.04.026.

[13] A. Mwesigye, J.P. Meyer, Optimal thermal and thermodynamic performance of a solar parabolic trough receiver with different nanofluids and at different concentration ratios, Appl. Energy. 193 (2017) 393–413. https://doi.org/10.1016/j.apenergy.2017.02.064.

[14] A. Allio, R. Difonzo, A. Leggieri, F. Legrand, R. Marchesin, L. Savoldi, Test and Modeling of the Hydraulic Performance of High-Efficiency Cooling Configurations for Gyrotron Resonance Cavities, Energies . 13 (2020). https://doi.org/10.3390/en13051163.

[15] L. Savoldi, A. Allio, A. Bovento, M. Cantone, J. Fernandez Reche, Experimental and numerical investigation of a porous receiver equipped with Raschig Rings for CSP applications, Sol. Energy. (2020).

[16] M. Cantone, M. Cagnoli, J. Fernandez Reche, L. Savoldi, One-side heating test and modeling of tubular receivers equipped with turbulence promoters for solar tower applications, Appl. Energy. 277 (2020) 115519. https://doi.org/https://doi.org/10.1016/j.apenergy.2020.115519.

[17] E. Kaloudis, E. Papanicolaou, V. Belessiotis, Numerical simulations of a parabolic trough solar collector with nanofluid using a two-phase model, Renew. Energy. 97 (2016) 218–229. https://doi.org/https:// doi.org/10.1016/ j.renene.2016.05.046.

[18] S.P.S. Inc.:, Star-CCM+ User's Guide v 14.02, (2019).

[19] R. Aguilar, L. Valenzuela, A.L. Avila-Marin, P.L. Garcia-Ybarra, Simplified heat transfer model for parabolic trough solar collectors using supercritical CO2, Energy Convers. Manag. 196 (2019) 807–820. https://doi.org/https://doi.org/10.1016/j.enconman.2019.06.029.

[20] A.G. Dixon, G. Walls, H. Stanness, M. Nijemeisland, E.H. Stitt, Experimental validation of high Reynolds number CFD simulations of heat transfer in a pilot-scale fixed bed tube, Chem. Eng. J. 200–202 (2012) 344–356. https://doi.org/https://doi.org/10.1016/j.cej.2012.06.065.

[21] T.-H. Shih, W.W. Liou, A. Shabbir, Z. Yang, J. Zhu, A new k-ϵ eddy viscosity model for high reynolds number turbulent flows, Comput. Fluids. 24 (1995) 227–238. https://doi.org/https://doi.org/10.1016/0045-7930(94)00032-T.

[22] T.M. Soe, S.Y. Khaing, Comparison of Turbulence Models for Computational Fluid Dynamics Simulation of Wind Flow on Cluster of Buildings in MandalayNo Title, Int. J. Sci. Res. Publ. 7 (2017) 337–350.

[23] E.M. Moghaddam, E.A. Foumeny, A.I. Stankiewicz, J.T. Padding, Heat transfer from wall to dense packing structures of spheres, cylinders and Raschig rings, Chem. Eng. J. 407 (2021) 127994. https://doi.org/https://doi.org/10.1016/j.cej.2020.127994.

[24] Y. Dong, B. Sosna, O. Korup, F. Rosowski, R. Horn, Investigation of radial heat transfer in a fixed-bed reactor: CFD simulations and profile measurements, Chem. Eng. J. 317 (2017) 204–214. https://doi.org/https://doi.org/10.1016/j.cej.2017.02.063.

[25] E. Bellos, C. Tzivanidis, Investigation of a star flow insert in a parabolic trough solar collector, Appl. Energy. 224 (2018) 86–102. https://doi.org/https://doi.org/10.1016/j.apenergy.2018.04.099.

[26] B.N. Kumar, K.S. Reddy, Numerical investigations on metal foam inserted solar parabolic trough DSG absorber tube for mitigating thermal gradients and enhancing heat transfer, Appl. Therm. Eng. 178 (2020) 115511. https://doi.org/https://doi.org/10.1016/j.applthermaleng.2020.115511.

[27] İ.H. Yılmaz, A. Mwesigye, T.T. Göksu, Enhancing the overall thermal performance of a large aperture parabolic trough solar collector using wire coil inserts, Sustain. Energy Technol. Assessments. 39 (2020) 100696. https://doi.org/https://doi.org/10.1016/j.seta.2020.100696.

[28] A. Mwesigye, T. Bello-Ochende, J.P. Meyer, Heat transfer and thermodynamic performance of a parabolic trough receiver with centrally placed perforated plate inserts, Appl. Energy. 136 (2014) 989–1003. https://doi.org/https://doi.org/10.1016/j.apenergy.2014.03.037.

[29] E. Bellos, C. Tzivanidis, D. Tsimpoukis, Thermal enhancement of parabolic trough collector with internally finned absorbers, Sol. Energy. 157 (2017) 514–531. https://doi.org/https://doi.org/10.1016/j.solener.2017.08.067.